

Injection and nucleation of topological defects in the quench dynamics of the Frenkel-Kontorova model

Oksana Chelpanova¹, Shane P. Kelly¹, Giovanna Morigi², Ferdinand Schmidt-Kaler¹ and Jamir Marino¹

¹*Institut für Physik, Johannes Gutenberg-Universität Mainz, D-55099 Mainz, Deutschland*

²*Theoretische Physik, Universität des Saarlandes, D-66123 Saarbrücken, Deutschland*

(Dated: October 27, 2022)

We explore the dynamics of a commensurate-incommensurate (C-IC) transition in a one-dimensional model described by the Frenkel-Kontorova model. An incommensurate ratio of the period of the trapping potential and the average inter-particle distance triggers a rearrangement of the atoms in a configuration where they can stably occupy positions dislocated from the potential minima. We show that the transition mirrors in non-equilibrium dynamics by unveiling a phenomenon of discrete injection of atomic dislocations, entering in a ‘step-wise’ fashion from the edges of the chain. Furthermore, we show that by quenching the system at the boundary of the C-IC transition, these discommensurations can be nucleated by thermal or quantum fluctuations, resulting in a dynamical regime with non-integer number of dislocations. Our work offers perspectives for exploring dynamical responses with topological character in trapped ions experiments.

Introduction.— The theme of solitons is interdisciplinary and permeates different areas of physics. They are a resource for quantum computing [1–4], cold atoms [5–8], atomic sensors [9–11], encompassing emergent dynamics in spintronics [12–14], and nano-friction in material science [15–20].

The Frenkel-Kontorova model [21, 22] offers a description of kinks in one-dimensional systems [23, 24] in terms of local discommensurations of particles in a periodic substrate potential, and it serves as archetypal model for several systems hosting solitons [24, 25]. Such discommensurations emerge as a result of a structural first-order transition from a (topologically trivial) commensurate state, in which particles stay at the minima of an underlying periodic potential, to an incommensurate state, where particles are dislocated from their natural equilibria. The incommensurate configurations can be mapped into solitons of a one-dimensional crystalline field ruled by a Sine-Gordon theory [24–28].

In this Letter, we promote the Frenkel-Kontorova model as a platform to tailor and control the injection of solitons in variety of quantum simulators, with special focus on trapped ions. Specifically, we show that kinks in the one-dimensional Frenkel-Kontorova model can be injected from the boundaries of the system by performing quenches which originate from the commensurate phase. This mechanism occurs in a controlled fashion with atomic discommensurations entering the chain at discrete intervals of time and building a metastable state characterized by a temporal staircase of kinks, with life-time scaling linearly with the chain size.

We also explore the impact of non-equilibrium fluctuations at the C-IC transition, and show that they can mold novel states in the quantum Frenkel-Kontorova model. In fact, by quenching the system close to the boundary of the C-IC transition, quantum fluctuations lead to statistical nucleation of kinks, which drive the chain in a quantum superposition of configurations with and without solitons. We focus through the paper on parameters regimes proper of trapped ions experiments,

although we lay out in the concluding sections a concrete plan to observe similar phenomena in low dimensional ultracold atomic wires, arguing for broad applicability of our results to other quantum simulators.

Model.— We consider N atoms forming a one-dimensional chain with inter-particle spacing a_0 . The system is subject to a periodic external lattice potential of period a_s . The physics of the discommensuration between the atoms spacing and the lattice periodicity can be captured by the Frenkel-Kontorova model [21, 22, 24–26]

$$H = \sum_n \frac{\dot{\phi}_n^2}{2} + m_K^2 (1 - \cos \phi_n) + \sum_{r=\pm 1} \frac{(\phi_{n+r} - \phi_n - 2\pi r \delta)^2}{2} \quad (1)$$

Here the first term describes the kinetic energy of the atoms, the second one depicts the interaction with the lattice potential, and the last term takes into account inter-particle interaction. Here $\phi_n/(2\pi) = x_n/a_s - n$ denotes a classical field, characterizing the displacement of the n -th particle position x_n from the coordinate of the n -th minima of the lattice potential ($n = 1, \dots, N$). The dimensionless parameter m_K captures the amplitude of the periodic lattice potential and it plays the role of the kink mass in the following. The ‘misfit parameter’ $\delta = (a_0 - a_s)/a_s$ quantifies instead the degree of discommensuration between a_0 and a_s . Due to the interplay between m_K and δ two different configurations for ϕ_n are possible. The equilibrium phase diagram is sketched in Fig. 1(a). For $\delta < \delta_c \approx 2m_K/\pi^2$ a strong lattice potential pins the particles to the potential minima, forming a commensurate phase ($\phi_n = \pi$), see Fig. 1(b, d). Instead, for values of $\delta \geq \delta_c$ atoms reside in a new incommensurate configuration associated with kinks in ϕ_n placed at the location of the particles’ displacements, cf. Fig. 1(b, c). Physically, kinks and anti-kinks describe respectively the local distribution of holes or excess of atoms in the chain [24–28]. Each kink (anti-kink) corresponds to a ‘step’ in the displacement field, ϕ_n , equal to 2π (-2π).

The number of kinks $Q = (\phi_N - \phi_1)/(2\pi)$ is a parameter that allows us to distinguish between the commensurate and the incommensurate phases [29]. This quantity estimates the number of ‘steps’ in ϕ_n , i.e., jumps in the value of the field ϕ from $\pi + 2\pi m$ to $\pi + 2\pi(m+1)$, where m is an integer number. For instance, the incommensurate configuration in Fig. 1(b, c) has three ‘steps’ in ϕ_n which corresponds to $Q = 3$. For large values of the misfit parameter δ , the number of kinks, Q , is linearly proportional to δ . Accordingly, Q is directly related to the spacing between kinks, $l_\delta \propto 1/\delta$. The width of the kink, l_m , is equal to the distance over which ϕ increases by 2π , and it is roughly proportional to the inverse of the kink mass, $l_m \propto 1/m_K$ [26, 29, 30]. For large m_K the shape of the kink is sharp, since any broadening of the incommensurate region requires additional energy cost due to the lattice potential. For small m_K the lattice potential is almost negligible and even a single kink appears wide.

The effective long-wavelength description of Eq. (1), is a sine-Gordon model with m_K controlling the strength of the non-linearity ($\sim m_K^2 \cos \phi$), and the misfit parameter δ coupling to the gradient of the field ($\sim \delta \partial_x \phi$). The latter is a chemical potential term which makes the solitons energetically preferred configurations for $\delta > \delta_c$. This model is known as Pokrovsky-Talapov field theory [29, 31, 32], and it finds numerous applications in solid state, cold atoms and statistical mechanics.

Following [29, 33] the excitation spectrum of the model (1) in the two phases can be extracted by expanding the equations of motion for ϕ_n around the classical solution $\phi_n^{(0)}$ in powers of small fluctuations η_n . The corresponding equations of motion for the linear displacements, η_q , in momentum space read

$$\omega_q^2 \eta_q = -m_K^2 \cos(\phi^0) \eta_q + c^2 q^2 \eta_q + \dots, \quad (2)$$

where c is the speed of sound, which we will set equal to one in the following, unless otherwise specified. The spectrum in the incommensurate phase consists of two branches, cf. Fig. 1(e). The first Q modes correspond to gapless collective excitations, phonons, describing the propagation of kinks through the lattice at the speed of sound c (blue line). The remaining $N - Q$ modes form an optical branch (red line) and they describe small harmonic displacements of the atoms around the potential minima: they are parabolically dispersing excitations with a gap set by m_K . Within the commensurate phase, all the N modes are optical.

The Hamiltonian (1) is a model description for discommensurations of ions confined by an optical lattice potential [17, 34–36]. In this realization, the inter-particle distance a_0 is controlled by the competition of the Coulomb repulsion between ions and an external Paul trap. The mass of the kink m_K is equal to the ratio of the amplitude of the lattice potential to the Coulomb repulsion between nearest ions. We detail the connection to the Frenkel-Kontorova in [37] and we simulate in the following the dynamics ruled by (1) in the parameters regime of a typical trapped ions experiment [34, 38].

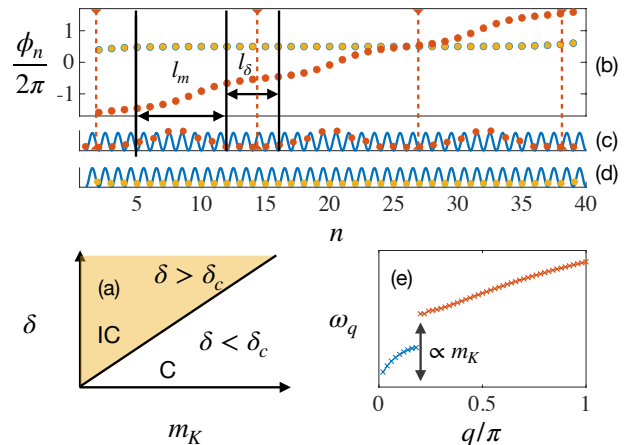


FIG. 1. (a) Equilibrium phase diagram of the model (1) as a function of the kink mass m_K and the misfit parameter δ . (b) Displacement, ϕ_n , of the n -th atom with respect to the n -th minimum of the potential for the incommensurate phase (red) and the commensurate phase (yellow). (c) Equilibrium positions of the atoms in the incommensurate phase. Some atoms sit at the minima of the lattice potential, while others in discommensurate equilibrium positions which can be mapped into kinks of ϕ_n (regions between red dashed lines in panel (b)). (d) The atomic positions in the commensurate phase coincide with the minima of the trapping potential. (e) Energy spectrum of the model as a function of momentum, q . Blue crosses correspond to sonic excitations, while red ones to parabolically dispersing modes (optical branch).

Dynamical response.— We investigate the dynamical response of the system by quenching the misfit parameter δ while keeping m_K fixed. We show that the transition from the commensurate to the incommensurate phase can be generated dynamically with an abrupt change of δ , from δ_i to δ_f and it is associated with the discrete injection of kinks from the edges of the chain into the bulk of the system. In fact, atoms in the bulk compensate discommensuration from left and right neighbours. Thus, merely atoms on the two boundaries are sensitive to the quench of δ and kinks are able to enter the system solely at these locations. In this scenario the outer part of the chain acts as a reservoir of solitons (see also [7, 39–41]). Furthermore, due to their topological nature, kinks can not be destroyed in the bulk [23, 42, 43]. In principle, an excitation of a kink–anti-kink pair is also topologically allowed, however, its energy cannot be accessed with the class of quenches considered here [34, 38, 44, 45].

In order to study dynamics, we numerically solve the equations of motion for ϕ_n without taking into account quantum fluctuations, which will be later incorporated in our analysis. In Fig. 2(a) we plot a diagram of the possible dynamical responses in the system using the long-time averaged number of kinks [46].

In the white region of Fig. 2(a) no kinks or anti-kinks

are produced during dynamics. The red region in the phase diagram corresponds to kinks' production after quenching the misfit parameter above a dynamical critical threshold, δ_c^d . Finally, the blue region in Fig. 2(a) corresponds to quenches which decrease the total number of kinks. This occurs by injecting anti-kinks into the system. Injection of a single kink (an anti-kink) from the boundary is associated with the excitation of a collective sonic mode.

Fig. 2(b) shows the time dependence of the number of kinks in the system after a quench from the commensurate to a target point of the incommensurate phase, marked with \star in Fig. 2(a). Dynamics start from $Q = 0$ and exhibit a staircase structure in time due to the injection of kinks from the boundaries up to time $\tau \propto N/c$ when finite-size effects become relevant. The duration of the various plateau of the staircase is proportional to l_{δ_f}/c . Arranging kinks at $r < l_\delta + l_m$ requires an additional energy cost. In order to show that, we calculate the energy of two kinks as a function of the relative distance between their centers r , cf. Fig. 2(c). If the kinks overlap, their energy is higher than the energy of the configuration with two infinitely separated kinks, resulting in short-distance repulsion [24, 47]. Thus, the average distance between kinks after the quench is fixed to approximately $l_m + l_{\delta_f}$. As a result, the number of kinks saturates at long times to $Q \approx N/(l_m + l_{\delta_f})$, which is basically given by the total number of solitons fitting in the system, for a given size N (cf. inset in Fig. 2(b)). Indeed, up to times τ , systems with a different number of particles evolve with the same staircase temporal profile, since dynamics are universally ruled by δ_f and m_K . Notice that the height of each 'step' in Fig. 2(b) is equal to two, since we simultaneously inject one kink from the left and another one from the right boundary, after the quench. Finally, on dynamical timescales longer than τ , optical modes start to dominate, resulting in oscillatory dynamics set by a frequency proportional to m_K .

The fact that we can separate kinks and define their velocities and shapes highlights that they behave as quasi-particles [23, 43]. Taking into account the long-range character of Coulomb repulsion leaves the results qualitatively unaltered as we discuss in [37].

Another way of triggering dynamical effects would be to perform a quench in m_K . Additionally to the effects discussed so far, a bound state of a kink and anti-kink can be excited in this case, as we present in detail in Ref. [44].

Dynamics close to the boundary of the C-IC transition.— Fluctuations can alter dynamics close to the boundary between two phases by destroying order, generating new dynamical phases, or provoking a 'blurring' transition in the system [48–55]. In the following we investigate the impact of quantum fluctuations on the results discussed so far by running semi-classical dynamics with the Truncated Wigner Approximation (TWA) [56–58]. First-order quantum corrections can be incorporated by adding quantum noise to the initial classical values of

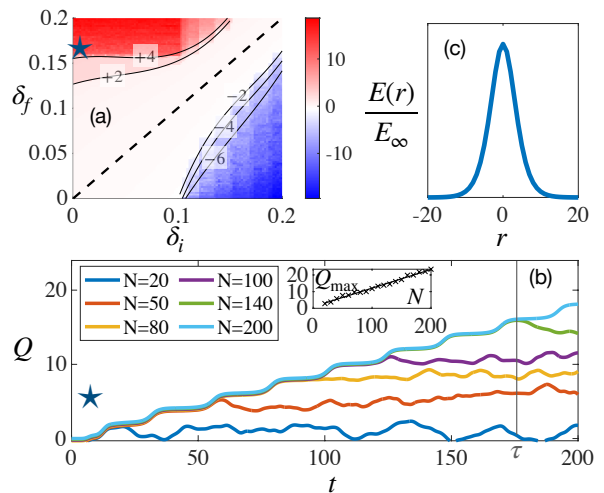


FIG. 2. (a) Dynamical response of the system after a quench of the misfit parameter from δ_i to δ_f , with $m_K = 0.5$ (here $N = 80$). We plot the time-averaged number of kinks, $\bar{Q} - Q_{(t=0)}$. The solid lines mark the critical thresholds, δ_c^d , corresponding to the discrete injection of a certain number of (anti-)kinks. The dashed line corresponds to $\delta_i = \delta_f$. The red region corresponds to the injection of kinks into the system, while the blue one pertains to anti-kinks. (b) Dynamics of the number of kinks in the system after the quench marked with a \star in panel (a). Here we fix $\delta_i = 0$ and $\delta_f = 0.16 > \delta_c^d$ and consider different system sizes N (marked with different colors). The plot illustrates periodic injection of kinks mirroring in a 'step-like' increase of Q in time. The time scale $\tau \propto N/c$ denotes the saturation time of Q for $N = 140$ ions after which finite-size effects take over. The maximal number of kinks in the system after the quench scales linearly with N (see inset). (c) Energy of two kinks as a function of the relative distance between their centers. Kinks repulsion takes place at distances $r < l_\delta + l_m$. The energy scale in panel (c) is normalized by the energy of two infinitely separated kinks E_∞ .

the field $\phi_n = \phi_n^{(0)} + \eta_n$, and to its conjugate momenta $p_n = p_n^{(0)} + n_n$, and then evolving equations of motion for several noise realizations. Observables can then be calculated by averaging the expectation value of operators over the trajectories resulting from initial quantum noise. The fluctuations η_n and n_n are sampled from a Gaussian Wigner quasi-probability distribution; their variances are reported in [37] and they are proportional to a (dimensionless) effective Planck constant $h_{\text{eff}} \propto (a_s^2 a_0^{3/2})^{-1}$ in the range of $10^{-5} \lesssim h_{\text{eff}} \lesssim 10^{-2}$ for the experimental parameters in [34]. Specifically, h_{eff} controls the accuracy in measuring the position and momentum of a single atom in the chain [17]. Taking into account higher orders quantum corrections can be performed by adding additional quantum jumps during dynamics, with each jump introducing $O(h_{\text{eff}}^2)$ corrections [56, 59].

Let us now revisit the quench of the misfit parameter within the commensurate phase, $\delta_i = 0 \rightarrow \delta_f \lesssim \delta_c^d$. At the classical level this excites the displacement field $\phi_n^{(0)}$

in an optical mode. At small times the dynamics of fluctuations are governed by $\ddot{\eta}_q \approx m_K^2 \cos(\phi^0(t)) \eta_q - c^2 q^2 \eta_q$ (cf. with Eq. (2)), with a periodically driven mass term set by the motion of $\phi_n^{(0)}(t)$. In cosmology [60] or cold atoms [61], a similar structure for dynamics of the low-energy modes results in an instability that can trigger non-linear effects. In our system the parametric amplification of low-energy modes can indeed cause the separation of quantum trajectories on times of order $\log h_{\text{eff}}$. Fig. 3(a) shows final configurations of the field for different samplings of the Wigner distribution associated to the pre-quench state. The yellow trajectories remain within the commensurate phase and contain no kinks, while the blue trajectories are the ones which have ‘tunnelled’ per effect of fluctuations into the incommensurate region, and in fact they display kinks in the profile of the displacement field, ϕ_n . After averaging over initial quantum noise (solid black line), the resulting ‘number of kinks’ Q takes a non-integer value (cf. Fig. 3(b)). In this sense, quantum fluctuations promote a new dynamical response with values of Q without counterpart at the mean-field level. We check that this result remains qualitatively unaltered after adding higher order quantum corrections in Fig. 3(b).

Fig. 3(c) portrays the energy of the system as a function of δ . Classically, a quench $\delta_i = 0 \rightarrow \delta_f \lesssim \delta_c^d$ keeps the system within the commensurate phase since the injection of a single kink would require an additional energy cost $\Delta E = E(\delta_c) - E(\delta_f)$. By adding quantum fluctuations, however, the system can tunnel through this barrier and nucleate a kink at the boundary. The transition probability can be calculated with the WKB approximation [62], considering the propagation of a ‘particle’ along the δ ‘direction’ tunneling through the barrier ΔE ; this yields the formula $P = P_0 \exp\left(-\alpha h_{\text{eff}}^{-1} \int_{\delta_f}^{\delta_c} \sqrt{E(\delta_c) - E(\delta)} d\delta\right)$, which we fit in good agreement with numerical results in the inset of Fig. 3(a). This also captures the fact that by performing a quench closer to the boundary between two phases δ_c^d , more final trajectories will contain a kink as they should climb smaller energy differences.

The effective Planck constant h_{eff} defines the width of the region in $\delta_c^d - \delta_f$ where separation of trajectories can be observed. For values of δ_f that are farther from δ_c^d , quantum noise provokes instead dephasing among trajectories. The overall result is that the width of a single kink will be broadened and the position of atoms will be harder to resolve.

As shown in the portrait of dynamical responses (Fig. 2(a)) there is a set of critical thresholds $\delta_{c_n}^d$ that correspond to the injection of multiple ($n = \pm 2, \pm 4, \dots$) solitons into the system. Therefore, by quenching δ in between $\delta_{c_n}^d$ and $\delta_{c_{n+2}}^d$ we can generate states which are in a superposition of n and $n + 1$ kinks.

Notice that sampling trajectories from an initial Gibbs distribution would have led to tunnelling by thermal activation [63], and it would have given rise qualitatively

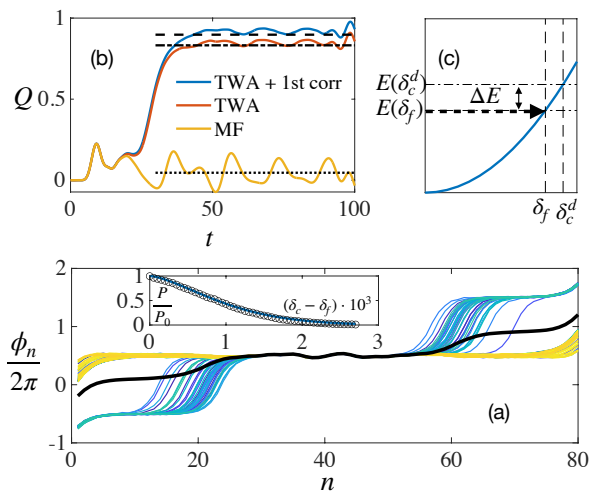


FIG. 3. (a) Separation of trajectories after a quench close to the boundary between two phases. Due to quantum fluctuations some final configurations contain a kink (blue) and some are commensurate (yellow), therefore the overall number of kinks in the averaged value of ϕ_n (solid black line), at long times, is non-vanishing. (b) Number of kinks as a function of time after the quench calculated classically (yellow), semi-classically (red), and taking into account next-order quantum corrections (blue). The dashed lines correspond to the time-averaged Q . The number of kinks at the classical level is zero and the system remains in the commensurate phase, while for TWA dynamics and for its first-order correction, the time-averaged Q takes a non-integer value between zero and one. (c) Energy of the system as a function of δ . The inset of panel (a) compares the probability of nucleating a kink through the energy barrier as a function of the final misfit parameter, for numerics from TWA (circles) and for the WKB approximation (solid); fitting parameters are $P_0 = 0.81$ and $\alpha = 5$.

to the same results of Fig. 3, with the major difference that the system would have been in a mixed state of crystal configurations with different values of Q .

Outlook.— In order to resolve commensurate and incommensurate configurations in trapped ions experiments, one could image the ions positions by applying non-destructive far-field measurements [64] using the diffractive pattern obtained from the scattered light. Alternatively, one could resort to AC-Stark shift methods [65] in order to distinguish the positions of the ions more accurately. Further experimental details such as the effect of the external Paul trap, and an estimate of the temperature required to observe quantum superpositions of kinks in trapped ions experiments are elaborated in [37].

As anticipated C-IC transitions are ubiquitous in a variety of platforms: ultra-cold gases [30, 45, 61, 66–69], trapped ions applied to nano-friction [15–17], cavity quantum electrodynamics [18, 70], magnetism [24, 25, 71, 72] and tangentially also strongly correlated systems [73, 74]. This naturally suggests broad applicability of our results to different platforms.

For instance, in the cold atoms implementation of Ref. [30], the Pokrovsky-Talapov model describes the dynamics of the phase difference between two Raman tunnel-coupled one-dimensional Bose quasi-condensates. The wave-vector difference of the Raman beams plays the role of the solitons chemical potential (δ in the model of Eq. (1)). Quantum quench dynamics would therefore become accessible through interferometric measurements of the correlation functions of the phase difference [75, 76].

This represents just one of the several interdisciplinary outreaches of our results which establish one more step towards merging the fields of topological defects and dynamical phase transitions in low-dimensional quantum simulators.

Acknowledgments – We thank Riccardo J. Valencia-Tortora for proof reading the manuscript and V. Vuletić for useful discussions. J. M. acknowledges E. Demler and V. Kasper for previous collaborations on related topics. This project has been supported by the Deutsche Forschungsgemeinschaft (DFG, German Research Foundation) – Project-ID 429529648 – TRR 306 QuCoLiMa (“Quantum Cooperativity of Light and Matter”), and by the Dynamics and Topology Centre funded by the State of Rhineland Palatinate and Topology Centre funded by the State of Rhineland Palatinate. The authors gratefully acknowledge the computing time granted on the supercomputer MOGON 2 at Johannes Gutenberg-University Mainz (hpc.uni-mainz.de).

-
- [1] C. Nayak, S. H. Simon, A. Stern, M. Freedman, and S. Das Sarma, Non-abelian anyons and topological quantum computation, *Rev. Mod. Phys.* **80**, 1083 (2008).
- [2] Y. Tokura, K. Yasuda, and A. Tsukazaki, Magnetic topological insulators, *Nature Reviews Physics* **1**, 126 (2019).
- [3] S. D. Sarma, M. Freedman, and C. Nayak, Topological quantum computation, *Physics today* **59**, 32 (2006).
- [4] H. Price, Y. Chong, A. Khanikaev, H. Schomerus, *et al.*, Roadmap on topological photonics, *Journal of Physics: Photonics* **4**, 032501 (2022).
- [5] L. Pitaevskii and S. Stringari, *Bose-Einstein Condensation and Superfluidity*, International series of monographs on physics (Oxford University Press, 2016).
- [6] A. Ramanathan, K. C. Wright, S. R. Muniz, M. Zelan, W. T. Hill, C. J. Lobb, K. Helmerson, W. D. Phillips, and G. K. Campbell, Superflow in a toroidal bose-einstein condensate: An atom circuit with a tunable weak link, *Phys. Rev. Lett.* **106**, 130401 (2011).
- [7] K. C. Wright, R. B. Blakestad, C. J. Lobb, W. D. Phillips, and G. K. Campbell, Driving phase slips in a superfluid atom circuit with a rotating weak link, *Phys. Rev. Lett.* **110**, 025302 (2013).
- [8] B. Damski and W. H. Zurek, Soliton creation during a bose-einstein condensation, *Phys. Rev. Lett.* **104**, 160404 (2010).
- [9] L. Amico, M. Boshier, G. Birkel, *et al.*, Roadmap on atomtronics: State of the art and perspective, *AVS Quantum Science* **3**, 039201 (2021).
- [10] T. Bland, I. Yatsuta, M. Edwards, Y. Nikolaieva, A. Olinyk, A. Yakimenko, and N. Proukakis, *Persistent current oscillations in a double-ring quantum gas* (2022).
- [11] S. Eckel, J. G. Lee, F. Jendrzejewski, N. Murray, C. W. Clark, C. J. Lobb, W. D. Phillips, M. Edwards, and G. K. Campbell, Hysteresis in a quantized superfluid ‘atomtronic’ circuit, *Nature* **506**, 200 (2014).
- [12] B. Göbel, I. Mertig, and O. A. Tretiakov, Beyond skyrmions: Review and perspectives of alternative magnetic quasiparticles, *Physics Reports* **895**, 1 (2021), beyond skyrmions: Review and perspectives of alternative magnetic quasiparticles.
- [13] B. J. Wieder, B. Bradlyn, J. Cano, Z. Wang, *et al.*, Topological materials discovery from crystal symmetry, *Nature Reviews Materials* **7**, 196 (2022).
- [14] E. Y. Vedmedenko, R. K. Kawakami, D. D. Sheka, *et al.*, The 2020 magnetism roadmap, *Journal of Physics D: Applied Physics* **53**, 453001 (2020).
- [15] L. Liu, M. Zhou, L. Jin, L. Li, Y. Mo, G. Su, X. Li, H. Zhu, and Y. Tian, Recent advances in friction and lubrication of graphene and other 2d materials: Mechanisms and applications, *Friction* **7**, 199 (2019).
- [16] A. Vanossi, C. Bechinger, and M. Urbakh, Structural lubricity in soft and hard matter systems, *Nature Communications* **11**, 1 (2020).
- [17] D. A. Gangloff, A. Bylinskii, and V. Vuletić, Kinks and nanofriction: Structural phases in few-atom chains, *Phys. Rev. Research* **2**, 013380 (2020).
- [18] T. Fogarty, C. Cormick, H. Landa, V. M. Stojanović, E. Demler, and G. Morigi, Nanofriction in cavity quantum electrodynamics, *Phys. Rev. Lett.* **115**, 233602 (2015).
- [19] T. Bohlein, J. Mikhael, and C. Bechinger, Observation of kinks and antikinks in colloidal monolayers driven across ordered surfaces, *Nature materials* **11**, 126 (2012).
- [20] L. Timm, H. Weimer, L. Santos, and T. E. Mehlstäubler, Energy localization in an atomic chain with a topological soliton, *Phys. Rev. Research* **2**, 033198 (2020).
- [21] Y. I. Frenkel and T. Kontorova, see phys. z. sowietunion 13 1, *Zh. Eksp. Teor. Fiz* **8**, 89 (1938).
- [22] F. C. Frank, J. H. van der Merwe, and N. F. Mott, One-dimensional dislocations. i. static theory, *Proceedings of the Royal Society of London. Series A. Mathematical and Physical Sciences* **198**, 205 (1949).
- [23] R. Rajaraman, Solitons and instantons. an introduction to solitons and instantons in quantum field theory. 1. reprint as a paperback (1987).
- [24] O. M. Braun and Y. S. Kivshar, *The Frenkel-Kontorova model: concepts, methods, and applications* (Springer, 2004).
- [25] P. Bak, Commensurate phases, incommensurate phases and the devil's staircase, *Reports on Progress in Physics* **45**, 587 (1982).
- [26] H. Landa, C. Cormick, and G. Morigi, Static kinks in chains of interacting atoms, *Condensed Matter* **5**, 10.3390/condmat5020035 (2020).
- [27] T. Pruttivarasin, M. Ramm, I. Talukdar, A. Kreuter, and H. Häffner, Trapped ions in optical lattices for prob-

- ing oscillator chain models, *New Journal of Physics* **13**, 075012 (2011).
- [28] I. García-Mata, O. Zhirov, and D. Shepelyansky, Frenkel-kontorova model with cold trapped ions, *The European Physical Journal D* **41**, 325 (2007).
- [29] D. N. Aristov and A. Luther, Correlations in the sine-gordon model with finite soliton density, *Phys. Rev. B* **65**, 165412 (2002).
- [30] V. Kasper, J. Marino, S. Ji, V. Gritsev, J. Schmiedmayer, and E. Demler, Simulating a quantum commensurate-incommensurate phase transition using two raman-coupled one-dimensional condensates, *Phys. Rev. B* **101**, 224102 (2020).
- [31] V. Pokrovsky and A. Talapov, Theory of incommensurate crystals, harwood acad, Publ., New York (1984).
- [32] V. L. Pokrovsky and A. L. Talapov, Ground state, spectrum, and phase diagram of two-dimensional incommensurate crystals, *Phys. Rev. Lett.* **42**, 65 (1979).
- [33] S. Marcovitch and B. Reznik, Entanglement of solitons in the frenkel-kontorova model, *Phys. Rev. A* **78**, 052303 (2008).
- [34] D. von Lindenfels, O. Gräß, C. T. Schmiegelow, V. Kaushal, J. Schulz, M. T. Mitchison, J. Goold, F. Schmidt-Kaler, and U. G. Poschinger, Spin heat engine coupled to a harmonic-oscillator flywheel, *Phys. Rev. Lett.* **123**, 080602 (2019).
- [35] R. B. Linnet, I. D. Leroux, M. Marciante, A. Dantan, and M. Drewsen, Pinning an ion with an intracavity optical lattice, *Phys. Rev. Lett.* **109**, 233005 (2012).
- [36] M. Cetina, A. Bylinskii, L. Karpa, D. Gangloff, K. M. Beck, Y. Ge, M. Scholz, A. T. Grier, I. Chuang, and V. Vuletić, One-dimensional array of ion chains coupled to an optical cavity, *New Journal of Physics* **15**, 053001 (2013).
- [37] See supplemental materials for the additional details related to the derivation of the effective model, reduction of the effective system size due to the external harmonic Paul trap, role of the long-range interaction and estimation of the critical temperature T_c .
- [38] Typical range of parameters for trapped-ion chain are $a_0 \in [5, 15] \mu\text{m}$, $N = 40 - 100$ ions, $\epsilon \in [0, 2\pi \cdot 2.7]$ MHz, $a_s = \lambda/(2 \cos \alpha)$ where $\lambda = 397\text{nm}$, $0 < \alpha < 22^\circ$; M is the mass of ^{40}Ca ions.
- [39] A. I. Yakimenko, Y. M. Bidasyuk, M. Weyrauch, Y. I. Kuriatnikov, and S. I. Vilchinskii, Vortices in a toroidal bose-einstein condensate with a rotating weak link, *Phys. Rev. A* **91**, 033607 (2015).
- [40] B. A. Kochetov, O. G. Chelpanova, V. R. Tuz, and A. I. Yakimenko, Spontaneous and engineered transformations of topological structures in nonlinear media with gain and loss, *Phys. Rev. E* **100**, 062202 (2019).
- [41] X. Ma, B. Berger, M. Aßmann, R. Driben, T. Meier, C. Schneider, S. Höfling, and S. Schumacher, Realization of all-optical vortex switching in exciton-polariton condensates, *Nature communications* **11**, 1 (2020).
- [42] T. Dauxois and M. Peyrard, *Physics of Solitons* (Cambridge University Press, 2006).
- [43] J. Brox, P. Kiefer, M. Bujak, T. Schaetz, and H. Landa, Spectroscopy and directed transport of topological solitons in crystals of trapped ions, *Phys. Rev. Lett.* **119**, 153602 (2017).
- [44] O. Chelpanova, S. Kelly, F. Schmidt-Kaler, G. Morigi, and J. Marino, In preparation (2022).
- [45] V. Gritsev, A. Polkovnikov, and E. Demler, Linear response theory for a pair of coupled one-dimensional condensates of interacting atoms, *Phys. Rev. B* **75**, 174511 (2007).
- [46] Time averages are taken over several periods $\propto 2\pi/m_K$.
- [47] R. Carretero-González, L. Cisneros-Ake, R. Decker, G. Koutsokostas, D. Frantzeskakis, P. Kevrekidis, and D. Ratliff, Kink-antikink stripe interactions in the two-dimensional sine-gordon equation, *Communications in Nonlinear Science and Numerical Simulation* **109**, 106123 (2022).
- [48] S. Sachdev, Quantum phase transitions, *Physics world* **12**, 33 (1999).
- [49] R. M. Fernandes, P. P. Orth, and J. Schmalian, Intertwined vestigial order in quantum materials: Nematicity and beyond, *Annual Review of Condensed Matter Physics* **10**, 133 (2019).
- [50] E. Shimshoni, G. Morigi, and S. Fishman, Quantum zigzag transition in ion chains, *Phys. Rev. Lett.* **106**, 010401 (2011).
- [51] Y. N. Gornostyrev, M. I. Katsnelson, A. V. Kravtsov, and A. V. Trefilov, Fluctuation-induced nucleation and dynamics of kinks on dislocation: Soliton and oscillation regimes in the two-dimensional frenkel-kontorova model, *Phys. Rev. B* **60**, 1013 (1999).
- [52] E. Shimshoni, G. Morigi, and S. Fishman, Quantum structural phase transition in chains of interacting atoms, *Phys. Rev. A* **83**, 032308 (2011).
- [53] A. Lazarides, O. Tieleman, and C. Morais Smith, Pokrovsky-Talapov model at finite temperature: A renormalization-group analysis, *Phys. Rev. B* **80**, 245418 (2009).
- [54] A. Lerose, J. Marino, B. Žunkovič, A. Gambassi, and A. Silva, Chaotic dynamical ferromagnetic phase induced by nonequilibrium quantum fluctuations, *Phys. Rev. Lett.* **120**, 130603 (2018).
- [55] A. Lerose, B. Žunkovič, J. Marino, A. Gambassi, and A. Silva, Impact of nonequilibrium fluctuations on prethermal dynamical phase transitions in long-range interacting spin chains, *Phys. Rev. B* **99**, 045128 (2019).
- [56] A. Polkovnikov, Phase space representation of quantum dynamics, *Annals of Physics* **325**, 1790 (2010).
- [57] R. Bistritzer and E. Altman, Intrinsic dephasing in one-dimensional ultracold atom interferometers, *Proceedings of the National Academy of Sciences* **104**, 9955 (2007).
- [58] D. X. Horváth, I. Lovas, M. Kormos, G. Takács, and G. Zaránd, Nonequilibrium time evolution and rephasing in the quantum sine-gordon model, *Phys. Rev. A* **100**, 013613 (2019).
- [59] J. Lancaster, E. Gull, and A. Mitra, Quenched dynamics in interacting one-dimensional systems: Appearance of current-carrying steady states from initial domain wall density profiles, *Phys. Rev. B* **82**, 235124 (2010).
- [60] P. B. Greene, L. Kofman, and A. A. Starobinsky, Sine-gordon parametric resonance, *Nuclear Physics B* **543**, 423 (1999).
- [61] C. Neuenhahn, A. Polkovnikov, and F. Marquardt, Localized phase structures growing out of quantum fluctuations in a quench of tunnel-coupled atomic condensates, *Phys. Rev. Lett.* **109**, 085304 (2012).
- [62] M. V. Berry and K. Mount, Semiclassical approximations in wave mechanics, *Reports on Progress in Physics* **35**, 315 (1972).
- [63] L. E. Reichl, A modern course in statistical physics (1999).

- [64] S. Wolf, J. Wechs, J. von Zanthier, and F. Schmidt-Kaler, Visibility of young's interference fringes: Scattered light from small ion crystals, *Phys. Rev. Lett.* **116**, 183002 (2016).
- [65] C. T. Schmiegelow, H. Kaufmann, T. Ruster, J. Schulz, V. Kaushal, M. Hettrich, F. Schmidt-Kaler, and U. G. Poschinger, Phase-stable free-space optical lattices for trapped ions, *Phys. Rev. Lett.* **116**, 033002 (2016).
- [66] I. Lovas, R. Citro, E. Demler, T. Giamarchi, M. Knap, and E. Orignac, Many-body parametric resonances in the driven sine-gordon model, *Phys. Rev. B* **106**, 075426 (2022).
- [67] N. K. Whitlock and I. Bouchoule, Relative phase fluctuations of two coupled one-dimensional condensates, *Phys. Rev. A* **68**, 053609 (2003).
- [68] H. P. Büchler, G. Blatter, and W. Zwerger, Commensurate-incommensurate transition of cold atoms in an optical lattice, *Phys. Rev. Lett.* **90**, 130401 (2003).
- [69] E. Haller, R. Hart, M. J. Mark, J. G. Danzl, L. Reichsöllner, M. Gustavsson, M. Dalmonte, G. Pupillo, and H.-C. Nägerl, Pinning quantum phase transition for a luttinger liquid of strongly interacting bosons, *Nature* **466**, 597 (2010).
- [70] J. M. Muñoz, R. Sawant, A. Maffei, X. Wang, and G. Barontini, Realizing the frenkel-kontorova model with rydberg-dressed atoms, *Phys. Rev. A* **102**, 043308 (2020).
- [71] J.-S. Caux, F. H. L. Essler, and U. Löw, Dynamical structure factor of the anisotropic heisenberg chain in a transverse field, *Phys. Rev. B* **68**, 134431 (2003).
- [72] N. Chepiga, From kosterlitz-thouless to pokrovskytalapov transitions in spinless fermions and spin chains with next-nearest neighbour interactions, arXiv preprint arXiv:2209.10390 <https://doi.org/10.48550/arXiv.2209.10390> (2022).
- [73] D. N. Aristov, V. V. Cheianov, and A. Luther, Optical conductivity of one-dimensional doped hubbard-mott insulator, *Phys. Rev. B* **66**, 073105 (2002).
- [74] P. Lebowitz and M. J. Stephen, Properties of vortex lines in superconducting barriers, *Phys. Rev.* **163**, 376 (1967).
- [75] M. Gring, M. Kuhnert, T. Langen, T. Kitagawa, B. Rauer, M. Schreitl, I. Mazets, D. A. Smith, E. Demler, and J. Schmiedmayer, Relaxation and prethermalization in an isolated quantum system, *Science* **337**, 1318 (2012).
- [76] T. Schweigler, V. Kasper, S. Erne, I. Mazets, B. Rauer, F. Cataldini, T. Langen, T. Gasenzer, J. Berges, and J. Schmiedmayer, Experimental characterization of a quantum many-body system via higher-order correlations, *Nature* **545**, 323 (2017).
- [77] O. M. Braun, Y. S. Kivshar, and I. I. Zelenskaya, Kinks in the frenkel-kontorova model with long-range interparticle interactions, *Phys. Rev. B* **41**, 7118 (1990).
- [78] G. Morigi and S. Fishman, Dynamics of an ion chain in a harmonic potential, *Phys. Rev. E* **70**, 066141 (2004).
- [79] D. H. E. Dubin, Minimum energy state of the one-dimensional coulomb chain, *Phys. Rev. E* **55**, 4017 (1997).
- [80] M. R. Kamsap, C. Champenois, J. Pedregosa-Gutierrez, S. Mahler, M. Houssin, and M. Knoop, Experimental demonstration of an efficient number diagnostic for long ion chains, *Phys. Rev. A* **95**, 013413 (2017).
- [81] A. Streltsov, G. Adesso, and M. B. Plenio, Colloquium: Quantum coherence as a resource, *Rev. Mod. Phys.* **89**, 041003 (2017).
- [82] S. P. Kelly, U. Poschinger, F. Schmidt-Kaler, M. P. A. Fisher, and J. Marino, *Coherence requirements for quantum communication from hybrid circuit dynamics* (2022).
- [83] K. Huang, *Introduction to statistical physics* (Chapman and Hall/CRC, 2009).
- [84] T. Cover and J. Thomas, *Elements of Information Theory* (Wiley, 2012).

Supplemental Material:
Injection and nucleation of topological defects
in the quench dynamics of the Frenkel-Kontorova model

Oksana Chelpanova¹, Shane P. Kelly¹, Giovanna Morigi², Ferdinand Schmidt-Kaler¹ and Jamir Marino¹

¹*Institut für Physik, Johannes Gutenberg-Universität Mainz, D-55099 Mainz, Deutschland*

²*Theoretische Physik, Universität des Saarlandes, D-66123 Saarbrücken, Deutschland*

Appendix A: Mapping trapped ions physics to the Frenkel-Kontorova model

The minimal model describing the trapped ion chain has Hamiltonian

$$H = K + V_{\text{int}} + V_{\text{lat}}. \quad (\text{A1})$$

Here the kinetic energy reads $K = M/2 \sum_n \dot{x}_n^2$, where M is the mass of the ions and x_n denotes the position of n -th ion. The Coulomb interaction between ions is equal to $V_{\text{int}} = 1/(4\pi\epsilon_0) \sum_{i,j>i} e^2/|x_i - x_j|$, where ϵ_0 is the vacuum's permittivity and e is an electron charge. The Coulomb repulsion can be expanded in the displacements around the equilibrium positions of ions $x_n^{(0)} = na_0$ that results in $V_{\text{int}} \approx \sum_n \sum_{r>0} K (x_{n+r} - x_n - ra_0)^2 / (2r^{m+2})$ with the spring constant $K = 2e^2 / (4\pi\epsilon_0 a_0^3)$. Fixing $m = \infty$ corresponds to taking into account only the short-range interaction ($r = 1$), while the $m = 1$ case describes the long-range interaction between ions [26, 77]. The last term in Eq. (A1) describes the potential energy of ions in the periodic lattice and reads as $V_{\text{lat}} = \epsilon \sum_n (1 - \cos(2\pi x_n/a_s)) / 2$. Here ϵ is the amplitude and a_s is the periodicity of the lattice potential. Let us introduce a dimensionless displacement of ion n from the position of the n -th potential minima as $\theta_n = 2\pi(x_n/a_s - n)$ and a dimensionless time $\tau = t\sqrt{K/M}$ for which the Hamiltonian reads

$$\tilde{H} = \frac{(2\pi)^2 H}{K a_s^2} = \sum_n \frac{1}{2} \dot{\theta}_n^2 + m_K^2 (1 - \cos \theta_n) + \sum_{r>0} \frac{1}{2|r|^{m+2}} ((\theta_{n+r} - \theta_n) - 2\pi r \delta)^2.$$

Here we have introduced a misfit parameter $\delta = a_0/a_s - 1$ that defines discommensurability between ions spacings and the lattice periodicity; the mass of the kink $m_K^2 = (2\pi)^2 \epsilon / (2K a_s^2)$ sets the amplitude of the lattice potential with respect to the Coulomb repulsion between nearest ions.

For the experimental parameters in [38] δ is always greater than one, which means that ions are always separated by few empty lattice sites. Let us exclude extra periodicity and parameterize variables as

$$\phi_n = \theta_n - \frac{2\pi}{\beta} [\delta] n + \pi \quad (\text{A2})$$

where $[\delta]$ denotes an integer part of δ , and also replace in the Hamiltonian the misfit parameter with its non-integer part $\delta = \{\delta\}$. This yields the Hamiltonian

$$\tilde{H} = \sum_n \frac{1}{2} \dot{\phi}_n^2 + m_K^2 (1 + \cos \phi_n) + \sum_{r>0} \frac{1}{2|r|^{m+2}} ((\phi_{n+r} - \phi_n) - 2\pi r \delta)^2, \quad (\text{A3})$$

which is the model discussed in the main text. The equation of motion that governs dynamics of the displacement ϕ_n reads

$$\ddot{\phi}_n = m_K^2 \sin \phi_n + \sum_{r \neq 0} \frac{1}{|r|^{m+2}} (\phi_{n+r} - \phi_n - 2\pi r \delta). \quad (\text{A4})$$

The dimensionless variables can be changed within the range $0 < m_K \lesssim 1.1$, $|\delta| < 0.5$ and $N \leq 100$ for the experimental parameters in [34].

In order to go beyond classical simulations we calculate semi-classical dynamics via the Truncated Wigner approximation [56, 57, 59]. Quantum operators are mapped to phase space variables which are sampled via the Wigner distribution. The time evolution of operators is then evaluated by running dynamics for each initial condition and averaging observables over these different trajectories. The Wigner distribution is defined as $W(\eta, n) = \int d\xi \langle \eta - \xi/2 | \hat{\rho} | \eta + \xi/2 \rangle e^{in\xi/\hbar}$ where η and n are vectors of phase space variables; here by $\hat{\rho}$ we denote the pre-quench density matrix. In the main text, we consider a quench from the ground state of the model (2), for which the Wigner function is equal to [56]

$$W(\eta_q^0, n_q^0) = \prod_q \exp \left[-|\eta_q^0|^2 / (2\sigma_q^2) - |n_q^0|^2 / (2b_q^2) \right], \quad (\text{A5})$$

where $b_q = h_{\text{eff}}/2\sigma_q$ and $\sigma_q = \sqrt{h_{\text{eff}}/2\omega_q}$. Here, the dispersion relation $\omega_q(q)$ is defined by Eq.(2) in the main text, and the effective Planck constant $h_{\text{eff}} = \hbar(2\pi)^2/a_s^2\sqrt{(4\pi\epsilon_0)a_0^3/(2e^2M)}$ controls the strength of quantum fluctuations. In the main text, the semi-classical observables are evaluated by averaging expectation values of operators over 10^3 trajectories, for which the initial conditions are sampled according to (A5).

Appendix B: Effect of an external Paul trap in trapped ions implementation

In the vicinity of the lattice potential the positions of ions $x_n^{(0)}$ are determined by the competition between the Coulomb repulsion and the external harmonic Paul trap. As a result, the spacing between ions a_0 is position-dependent and the effective number of ions, for which C-IC transition can be observed, is reduced. It has been shown [78–80] that, due to the competition between the Coulomb repulsion and an external harmonic trap, the spacing between ions has the following position dependence $a_0(x_i) = 1/n_L(x_i)$, where the density of ions is equal to $n_L(x_i) = 3N/(4L)(1 - x_i^2/L^2)$ and the total length of the system reads as $L^3 = 2q^2N \log N/(m\omega_0^2)$. Here q is an electron charge. The closer we are to the middle of the chain, the smaller difference in spacing a_0 is. We can require the deviations in ions spacing to be much smaller than a_s and keep the misfit parameter δ roughly fixed via $(a_0(x_{i+1}) - a_0(x_i))/a_s = \alpha \ll 1$. Then, the length of this region is equal to $l_s = L\sqrt{3N\alpha a_s/(4L + 3N\alpha a_s)}$ and the number of ions within it can be calculated as

$$s = \int_{-l_s}^{l_s} n_L(x) dx = \frac{3N}{2} \sqrt{\frac{3N\alpha a_s}{4L + 3N\alpha a_s}} \left(1 - \frac{N\alpha a_s}{4L + 3N\alpha a_s}\right) \quad (\text{B1})$$

Fig. 4(a) shows the size of this region as a function of N for $\alpha = 0.025$. Here, the dynamics of s ions in the center of the chain is governed by the Frenkel-Kontorova model and the usual C-IC transition is expected. For the parameters [38] and $N = 100$ only $s = 3$ ions in the center are equidistant, while for $N = 1000$ the effective system size $s = 60$. However, by increasing $N > 100$ ‘zigzag’ effects start to contribute, and atoms do not form a one-dimensional chain anymore, but start to deviate towards the direction perpendicular to the chain; therefore, the model would require to take into account an additional spatial dimension [50, 52].

This issue can be solved if we modify a lattice potential period a_s by increasing the standing wave period. One can combine the two beams such that the standing wave is only in direction or exactly orthogonal to the trap axis, inducing only a force in the radial direction, or exactly opposite. By increasing a_s we can also increase the effective system size as $l_s \propto \sqrt{a_s}$ in the leading order for small α . Thus, we can obtain $s \approx 30$ for $N = 100$ ions, to observe the transition discussed in the main text.

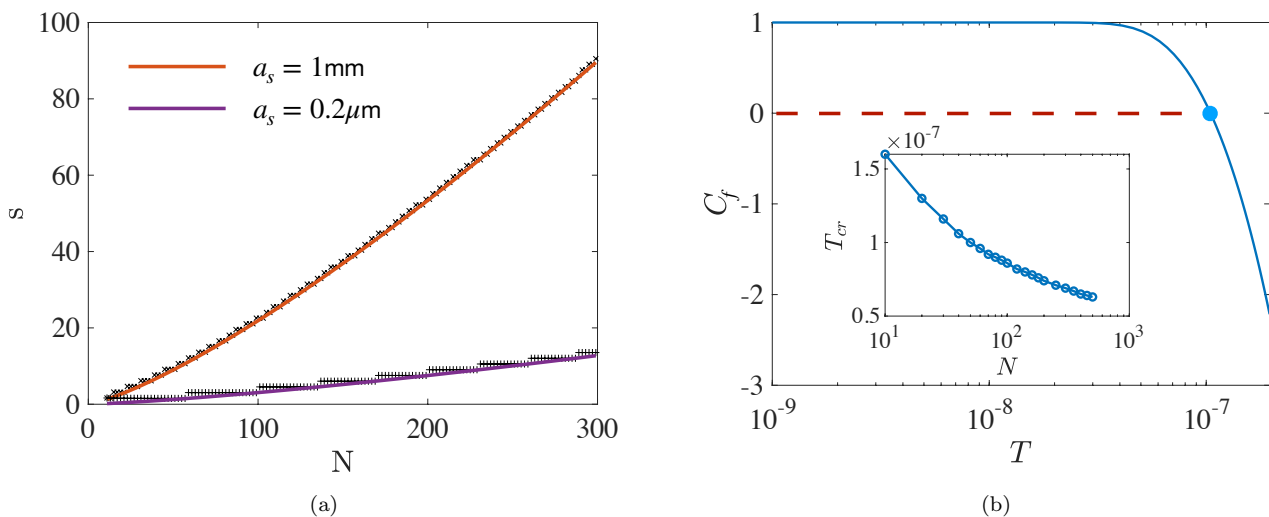


FIG. 4. (a) The effective size of the system as a function of the number of ions in the chain. Here we consider s ions in the middle of the lattice separated almost equidistantly in the absence of the periodic lattice potential. The violet line corresponds to the potential generated by two lasers crossed at an angle 22° (accessible in the current experiment [34]). The red line corresponds to the relative angle 89° . (b) Coherence of a system of $N = 10$ ions as a function of temperature. The blue dot shows the critical temperature below which quantum effects are washed out by thermal noise. The inset illustrates the critical temperature at which coherence vanishes as function of the system size.

Appendix C: Critical temperature

In this Appendix we use the relative entropy of coherence to determine an initial temperature range at which quantum fluctuations dominate over thermal ones, and a quantum superposition of state with and without a kink can be dynamically generated. The relative entropy of coherence is a quantifier for the resource theory of coherence [81–83] which encodes the amount of superposition a given state, ρ , has in a certain basis. If the basis has projectors $P_d = |d\rangle\langle d|$, then the relative entropy of coherence is written as

$$C(\rho) = S\left(\sum_d P_d \rho P_d\right) - S(\rho), \quad (\text{C1})$$

where $S(\rho)$ is the von Neumann entropy of the state ρ . Importantly, the state $\sum_d P_d \rho P_d$ has only diagonal entropies with weights equal to the probability $P(d) = \langle d|\rho|d\rangle$ of a measurement in the basis obtaining the outcome d . Thus, we find that $S(\sum_d P_d \rho P_d)$ is equal to the Shannon entropy, $H(P(d))$, of the distribution $P(d)$. The relative entropy of coherence is then simply the difference between the entropy of the classical distribution $P(d)$ and that of the quantum state ρ . If the quantum state is pure, we have $S(\rho) = 0$, and all entropy in $P(d)$ is due to superposition such that $C(\rho) = H(P(d))$; on the other hand if the state is mixed, some of the entropy in $P(d)$ is simply due to the mixed nature of the state ρ , and $C(\rho) < H(P(d))$.

In the main text, we demonstrated a way of generating uncertainty in the number of solitons, Q , present in the system. Since $Q = (\phi_N - \phi_1)/(2\pi)$, then we should investigate the coherence in a basis such that the observables $\hat{\phi}_i$ are diagonal: $\hat{\phi}_j |\{\phi_i\}\rangle = \phi_j |\{\phi_i\}\rangle$. After the system evolves the statistical mixture of states with and without a soliton, it will have some distribution $P(\{\phi_i\})$, for which we will want to identify how much entropy is due to superposition or a classical mixture of states: $C(\rho) = H(P(\{\phi_i\})) - S(\rho)$.

While the Shannon entropy, $H(P(\{\phi_i\}))$, is inaccessible in TWA calculations due to a sampling complexity problem, we can provide a lower bound on it using a data processing inequality [84] applied to a statistical classifier, $f(\{\phi_i\}) \in (0, 1)$ which identifies if the state has zero or one soliton. The data processing inequality states $H(P(\{\phi_i\})) \geq H(P(f(\{\phi_i\}))) \equiv H(P(f))$ such that

$$C(\rho) \geq C_f \equiv H(P(f)) - S(\rho). \quad (\text{C2})$$

When $C_f = 1$, then the state is an equal superposition of a chain with and without a soliton, and can only occur when $S(\rho) = 0$ (the initial state of the system is pure and the evolution over time is unitary). While C_f drops below zero when initial state thermal fluctuations dominate and $S(\rho) > 1$

We compute $H(P(f))$ from $P(f=1) = 1 - P(f=0)$ obtained by counting the fraction of TWA trajectories with and without a soliton. To compute $S(\rho)$, we assume the initial state is in some thermal Gibbs state $\rho_0 \sim e^{-\beta H}$ and undergoes strictly unitary evolution $\rho = U_t \rho_0 U_t^\dagger$ where U_t is the unitary generated by the Hamiltonian in Eq. 1. The entropy of the state ρ is then equivalent to the thermal entropy, and can be evaluated as $S = -\sum_q \rho_q \log \rho_q$ [83], where $\rho_q = e^{-\beta H_q}/Z_q$ is the reduced density matrix for mode q , β is the inverse temperature and Z_q is a normalization factor. For each mode q (2) we have

$$Z_q = \text{tr} \exp(-\beta H_q) = \text{tr} \exp\left(-\beta h_{\text{eff}} \omega_q \left(n_q + \frac{1}{2}\right)\right) = \frac{e^{-\beta h_{\text{eff}} \omega_q / 2}}{1 - e^{-\beta h_{\text{eff}} \omega_q}},$$

and after evaluating $\rho_{q,n} = e^{-\beta h_{\text{eff}} \omega_q n_q} (1 - e^{-\beta h_{\text{eff}} \omega_q})$ the thermal entropy reads

$$S(\rho) = \frac{h_{\text{eff}} \omega_q}{k_B T} \langle n_q \rangle - \log(1 - e^{-\beta h_{\text{eff}} \omega_q})$$

with $\langle n_q \rangle = (e^{\beta h_{\text{eff}} \omega_q} - 1)^{-1}$.

In Fig. 4(b) we show the typical dependence of coherence as a function of the temperature of the system for trapped ions implementation of the Frenkel-Kontorova model. For small temperatures $C_f \approx 1$, we know thermal entropy can not account for the statistical entropy of finding a state with and without a kink, and we conclude that the statistical uncertainty is due to superposition. Above a certain temperature scale T_{cr} , C_f drops below zero indicating the state is dominated by thermal fluctuations. For $N = 10$ ions, the critical temperature is equal to $T_{\text{cr}} = 0.1 \mu\text{K}$. The inset of Fig. 4(b) illustrates the scaling of critical temperature with the system size. Thermal entropy grows linearly with the system size, thus, at fixed temperature more quantum information is preserved in a system of smaller length. The critical temperature can be increased by enlarging the strength of quantum fluctuations $\propto h_{\text{eff}}$ at time $t = 0$ or by enhancing a driving mass term for quantum fluctuations n_q by increasing m_K , see Eq. (2) in the main text.

Appendix D: Long-range interactions

In this Appendix, we study the impact of long-range interactions on the properties of the ion chain and discuss the generality of the results in the main text. Taking into account Coulomb interactions between ions ($m = 1$ in Eq. (A3)) increases their mutual repulsion and it widens the length of a single kink l_m [26, 77]. Furthermore, as all ions are sensitive to the presence of dislocations, these will propagate faster along the system, while for short-range interactions only nearest neighbours are sensitive to the presence of dislocations and any local rearrangement spreads through the system at the speed of sound. Nonetheless, as we show below, the results in the main text remain qualitatively similar.

In Fig. 5(a) we reproduce Fig. 2(b) from the main text, which shows the temporal dependence of the number of kinks in the system after the quench, for a chain with Coulomb repulsion. Results remain qualitatively the same: kinks enter the system one by one from the boundaries. Quantitatively, the duration of the plateau is shortened as the form of a single kink is broadened by the Coulomb repulsion. Finite size effects start to build up at times $\tau \approx N/2c$, while in the short-range interacting system it takes approximately twice longer.

The role of Coulomb repulsion can be effectively suppressed by increasing m_K , whose inverse sets its relative strength with respect to the lattice potential. In this case, a staircase structure in $Q(t)$ can be observed more clearly, cf. Fig. 5 (b) for $m_K = 1$. In both cases, the maximal number of kinks in the system scales linearly with the system size which is also the case for the nearest-neighbour interactions, cf. insets in Fig. 5.

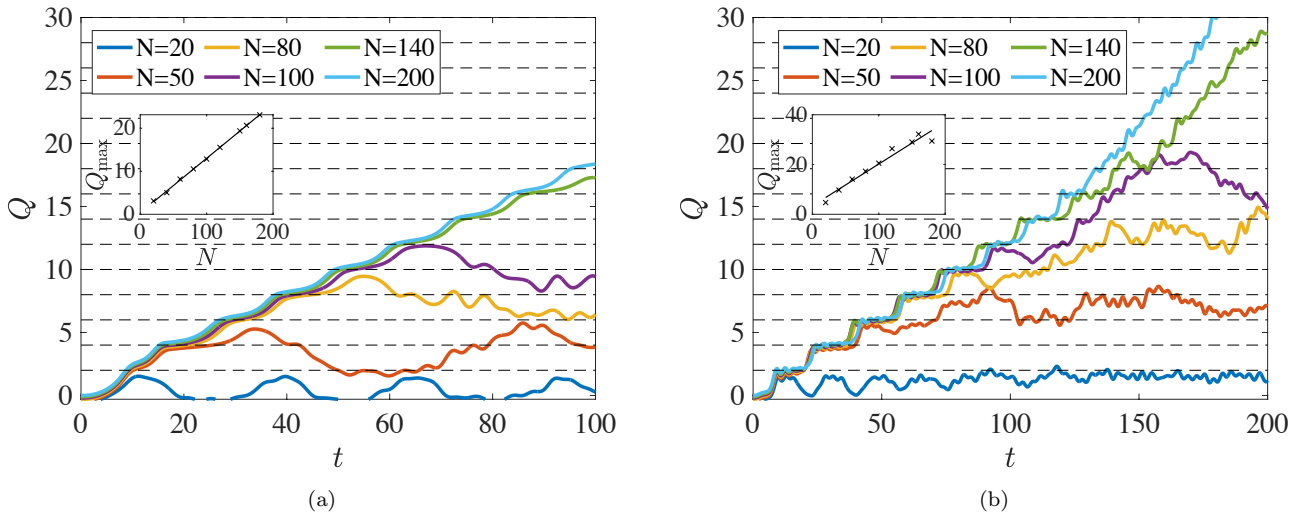


FIG. 5. Number of kinks in a chain with Coulomb interactions as a function of time for a quench from the commensurate to the incommensurate phase for (a) $m_K = 0.5$, $\delta_f = 0.12$ and (b) $m_K = 1$, $\delta_f = 0.2$. At $m_K = 0.5$ the Coulomb repulsion is stronger and this results in a broadening of the width of the kink, which yields a smoother staircase in $Q(t)$ in comparison with Fig. 2(b) of the main text. Increasing the mass of the kink to $m_K = 1$ suppresses the effect of Coulomb repulsion and kinks are sharper. Insets show the maximal number of kinks in the system as a function of the system size.